A Numerical Study of Static Bending of Reissner-Mindlin plate Using a Virtual Element Method

Xiaoxiao Du[1] 🆔 , Gang Zhao[2] , Wei Wang[3] , Jiaming Yang[4] , Mayi Guo[5] , Ran Zhang[6]

[1]Beihang University, duxiaoxiao@buaa.edu.cn
[2]Beihang University, zhaog@buaa.edu.cn
[3]Beihang University, jrrt@buaa.edu.cn
[4]Beihang University, williamyjm@163.com
[5]Beihang University, windowsgmy@126.com
[6]Beihang University, feliciamail@buaa.edu.cn

Corresponding author: Wei Wang, jrrt@buaa.edu.cn

Abstract. In this paper, we develop an arbitrary order virtual element method for the static bending analysis of Reissner-Mindlin plates. The transverse displacement and rotations are independently interpolated with the functions defined in the virtual element spaces. The interpolation functions for transverse displacement are one order higher than the functions for rotations. Due to the advantages of insensitivity to the elemental distortion and allowance of hanging nodes in the virtual element method, a simple mesh generation scheme is employed to generate polygonal mesh by using an initial background grid and a quadtree refinement approach. Some examples are studied to verify the accuracy and convergence of the developed method. The high convergence rates for transverse displacement and rotations could be observed from the numerical results.

1 INTRODUCTION

The virtual element method (VEM), introduced in [10] is designed for solving numerical problems defined on arbitrarily shaped polygonal/polyhedral discretizations. Therefore, it will greatly alleviate the heavy burden placed on meshing complex CAD geometries when compared with the traditional finite element method. Furthermore, VEM could handle the non-conforming discretizations by allowing the existence of hanging nodes, which are treated as normal nodes in the element. The local *h*-refinement and *p*-version refinement

could be easily implemented under the VEM framework. The shape functions are implicitly defined in VEM and all the integrations are obtained from a series of the predefined degree of freedoms. This is also the reason why the element is called "virtual" element. So far VEM has been successfully applied to solve various problems including topology optimization [7, 2], contact [18], fracture [17], plate bending and vibration [9, 8, 14], inelasticity [4].

Plate structures are widely used in practical engineering and the Reissner-Mindlin plate theory is a well-known assumption for the analysis of moderately thick plate structures. One of the main difficulties of this assumption is the "locking" phenomenon, frequently encountered when the thickness-length ratio is small. A variety of locking-free techniques have been proposed to solve this problem, e.g., reduced integration scheme [13], mixed interpolation technique [6], discontinuous Galerkin method [3], weak Galerkin method [19], isogeometric method [11]. Recently, VEM is also applied to solve the Reissner-Mindlin plate problem. Da Veiga et al, developed a variational formulation for Reissner-Mindlin plate considering the conforming approximation of shear strain and deflection [9]. Chinosi presented a virtual element method for bending analysis of Reissner-Mindlin plate following the MITC approach [8]. Note that the approaches proposed in [8, 9] are non-primary formulations by introducing a reduction operator or shear strain.

In this work, we developed a novel virtual element method for the bending problem of Reissner-Mindlin plate in the primary form on polygonal meshes following the approach proposed in [16, 19]. The primary form indicates that no shear strains or reduction operators are introduced. The degree of polynomials for interpolation of deflection is one-order higher than that of rotations to easily perform the integration calculation with the predefined degree of freedoms. The implementation procedures are simple and straightforward compared with the existing techniques. The mesh for VEM can be generated by using an initial background grid and a simple quadtree refinement scheme. Numerical results confirm the robustness and high convergence of the proposed method. It should be noticed that the bending results of thin plate are still suffered from the shear locking problems and further studies are opened.

2   REISSNER-MINDLIN PLATE PROBLEMS

Let Ω be the domain occupied by the middle plane of an elastic plate with thickness t. Let $\mathcal{W}$ and $\boldsymbol{\Theta}$ be the function spaces for the transverse displacement w and rotations $\boldsymbol{\theta}(\theta_x, \theta_y)$. Then the Reissner-Mindlin plate problems can be described as: Find $w \in \mathcal{W}, \boldsymbol{\theta} \in \boldsymbol{\Theta}$, such that

$$a(\boldsymbol{\theta}, \boldsymbol{\eta}) + b(\boldsymbol{\theta} - \nabla w, \boldsymbol{\eta} - \nabla v) = (g, v), \quad \forall (v, \boldsymbol{\eta}) \in \mathcal{W} \times \boldsymbol{\Theta}, \tag{1}$$

where the bilinear forms can be written as

$$a(\boldsymbol{\theta}, \boldsymbol{\eta}) = \int_{\Omega} \boldsymbol{\epsilon}^T(\boldsymbol{\theta}) \boldsymbol{D}_b \boldsymbol{\epsilon}(\boldsymbol{\eta}) d\Omega, \tag{2}$$

$$b(\boldsymbol{\theta} - \nabla w, \boldsymbol{\eta} - \nabla v) = \int_{\Omega} (\boldsymbol{\theta} - \nabla w)^T \boldsymbol{D}_s (\boldsymbol{\eta} - \nabla v) d\Omega, \tag{3}$$

in which $\boldsymbol{\epsilon}(\boldsymbol{\theta}) = 0.5(\nabla \boldsymbol{\theta} + \nabla \boldsymbol{\theta}^T)$ is the Voigt representation of the strain tensor. $\boldsymbol{D}_b$ and $\boldsymbol{D}_s$ are the material bending and shear constitutive matrices.

3   VIRTUAL ELEMENT METHOD

Let $\mathcal{T}_h$ be a decomposition of the domain Ω into a series of polygons. For each polygon $E \in \mathcal{T}_h$ and edge $e \in E$, the local VEM spaces of degree $k + 1(k \geq 1)$ for the transverse displacement w are defined as

$$\mathcal{W}_h^{k+1}(E) = \{w_h \in \mathcal{H}^1(E) : w_h|_e \in C^0(e), w_h|_E \in \mathcal{P}_{k+1}(E), \Delta w_h|_E \in \mathcal{P}_{k-1}(E)\} \tag{4}$$

with the associated degrees of freedom as follows

- Vertex DOFs: the values of w_h at each vertex of E;

- Edge DOFs: the values of w_h at k internal Gauss-Lobatto quadrature points on each edge of E;

- Face DOFs: the moments up to degree $k-1$ of w_h in E: $\dfrac{1}{|E|} \int_E w_h \cdot p dE, \forall p \in \mathcal{P}_{k-1}(E)$.

Let n_v be the number of vertices of the polygon E. The dimension of the space $\mathcal{W}_{h,E}^{k+1}$ is

$$dim(\mathcal{W}_h^{k+1}(E)) = n_v + kn_v + dim(\mathcal{P}_{k-1}(E)) = (k+1)n_v + \frac{k(k+1)}{2}. \tag{5}$$

Similarly, the local VEM spaces of degree k for rotations $\boldsymbol{\theta}$ can be given by

$$\boldsymbol{\Theta}_h^k(E) = \{\boldsymbol{\theta}_h \in [\mathcal{H}^1(E)]^2 : \theta_h^i|_e \in C^0(e), \theta_h^i|_E \in \mathcal{P}_k(E), \Delta\theta_h^i|_E \in \mathcal{P}_{k-2}(E), i = 1, 2\} \tag{6}$$

with the associated degrees of freedom as follows

- Vertex DOFs: the values of $\boldsymbol{\theta}_h$ at each vertex of E;

- Edge DOFs: the values of $\boldsymbol{\theta}_h$ at $k-1$ internal Gauss-Lobatto quadrature points on each edge of E;

- Face DOFs: the moments up to degree $k-2$ of $\boldsymbol{\theta}_h$ in E: $\dfrac{1}{|E|} \int_E \boldsymbol{\theta}_h \cdot \boldsymbol{p} dE, \forall \boldsymbol{p} \in \boldsymbol{\mathcal{P}}_{k-2}(E)$.

Then the dimension of the spaces $\boldsymbol{\Theta}_h^k$ is calculated as

$$dim(\boldsymbol{\Theta}_h^k(E)) = 2n_v + 2(k-1)n_v + 2dim(\mathcal{P}_{k-1}(E)) = 2kn_v + k(k-1). \tag{7}$$

Let Π_r^∇ be the local projection operator for vertical displacement, mapping the functions from the local space $\boldsymbol{\Theta}_h^k(E)$ to $\boldsymbol{\mathcal{P}}_k(E)$. Given $\boldsymbol{\theta}_h \in \boldsymbol{\Theta}_h^k(E)$, the projection operator Π_r^∇ satisfies:

$$a_h^E(\boldsymbol{\theta}_h, \boldsymbol{p}) = a_h^E(\Pi_r^\nabla \boldsymbol{\theta}_h, \boldsymbol{p}), \quad \forall \boldsymbol{p} \in \boldsymbol{\mathcal{P}}_k(E). \tag{8}$$

Assume that the function $\boldsymbol{\theta}_h$ could be expressed by the bases $\{\boldsymbol{\varphi}_i\}_{i=1}^{n_d}$ as $\boldsymbol{\theta}_h = \sum_{i=1}^{n_d} \boldsymbol{\varphi}_i \bar{\boldsymbol{\theta}}_i$, where n_d denotes the total number of basis functions, $\bar{\boldsymbol{\theta}}_i$ denotes the unknown rotations at ith DOF. Using the polynomial functions $\boldsymbol{p}_\alpha \in \boldsymbol{\mathcal{P}}_k(E)$ to express the projected function with $\Pi_r^\nabla \boldsymbol{\varphi}_i = \sum_{\alpha=1}^{n_k} \pi_{i,\alpha}^r \boldsymbol{p}_\alpha$, and combining Eqs. (2) and (8), a system of linear equation can be written as

$$a_h^E(\boldsymbol{\varphi}_i, \boldsymbol{p}_\beta) = \sum_{i=1}^{n_k} \pi_{i,\alpha}^r a_h^E(\boldsymbol{p}_\alpha, \boldsymbol{p}_\beta), \quad \forall \boldsymbol{p}_\beta \in \boldsymbol{\mathcal{P}}_k(E), \forall \boldsymbol{\varphi}_i \in \boldsymbol{\Theta}_h^k(E). \tag{9}$$

The right side term $a_h^E(\boldsymbol{p}_\alpha, \boldsymbol{p}_\beta)$ can be calculated directly and the left side term can be computed by using the rule of integration by parts as

$$a_h^E(\boldsymbol{\varphi}_i, \boldsymbol{p}_\beta) = \int_E \boldsymbol{\epsilon}^T(\boldsymbol{\varphi}_i) \boldsymbol{D}_b \boldsymbol{\epsilon}(\boldsymbol{p}_\beta) dE = -\int_E \boldsymbol{\varphi}_i^T \nabla \boldsymbol{D}_b \boldsymbol{\epsilon}(\boldsymbol{p}_\beta) dE + \int_e \boldsymbol{\varphi}_i^T \boldsymbol{D}_b \boldsymbol{\epsilon}(\boldsymbol{p}_\beta) \bar{\boldsymbol{n}} de, \tag{10}$$

where $\bar{\boldsymbol{n}}$ denotes the unit normal vector to the edges of E. Note that the integrand of the first term in the right side $\nabla \boldsymbol{D}_b \boldsymbol{\epsilon}(\boldsymbol{p}_\beta)$ could be expressed by using polynomials of degree $k-2$. Then we can compute the integration according to the predefined face DOFs. The integrand of the second term in the right side could be expressed by using polynomials of degree $2k-1$ and could be precisely calculated by using the $k+1$ Gauss-Lobatto quadrature points, namely the edge DOFs. Eventually, the coefficient $\boldsymbol{\pi}_r(\pi_{i,a})$ can be obtained by solving a

system of linear equations. Considering the orthogonality condition of the projection operator Π_r^∇, the bilinear form $a_h^E(\boldsymbol{\theta}_h, \boldsymbol{\eta}_h)$ is computed by

$$a_h^E(\boldsymbol{\theta}_h, \boldsymbol{\eta}_h) = a_h^E(\Pi_r^\nabla \boldsymbol{\theta}_h, \Pi_r^\nabla \boldsymbol{\eta}_h) + a_h^E(\boldsymbol{\theta}_h - \Pi_r^\nabla \boldsymbol{\theta}_h, \boldsymbol{\eta}_h - \Pi_r^\nabla \boldsymbol{\eta}_h), \tag{11}$$

where the first term is called consistent term and the second term is called stability term. Combining Eqs. (2) and (8), the consistent term can be written as

$$a_h^E(\Pi_r^\nabla \boldsymbol{\theta}_h, \Pi_r^\nabla \boldsymbol{\eta}_h) = \bar{\boldsymbol{\theta}}^T \boldsymbol{\pi}_r^T \left\{ \int_E (\boldsymbol{\partial} \boldsymbol{N}_p^r)^T \boldsymbol{D}_b (\boldsymbol{\partial} \boldsymbol{N}_p^r) dE \right\} \boldsymbol{\pi}_r \bar{\boldsymbol{\eta}} = \bar{\boldsymbol{\theta}}^T \boldsymbol{K}_a^c \bar{\boldsymbol{\eta}}, \tag{12}$$

and the stability stiffness matrix derived from the stability term is written as

$$\boldsymbol{K}_a^s = \tau tr(\boldsymbol{K}_a^c)(\boldsymbol{I} - \boldsymbol{D}_r \boldsymbol{\pi}_r)^T (\boldsymbol{I} - \boldsymbol{D}_r \boldsymbol{\pi}_r), \tag{13}$$

in which τ is a positive real number and is chosen as $\tau = 0.5$ according to the recommendation given in [5]. The matrix $\boldsymbol{D}_r$ is constituted by the value of polynomials $\boldsymbol{p}_j$ at i-th DOFs as $\boldsymbol{D}_r^{ij} = dof_i(\boldsymbol{p}_j)$. $\boldsymbol{\partial}$ is the gradient matrix and $\boldsymbol{N}_p^r$ is the matrix consisting of polynomials $\boldsymbol{p}_j$.

Next we consider the discrete bilinear form $b_h^E(\boldsymbol{\theta} - \nabla w, \boldsymbol{\eta} - \nabla v)$, which can be expanded as

$$b_h^E(\boldsymbol{\theta} - \nabla w, \boldsymbol{\eta} - \nabla v) = b_h^E(\nabla w, \nabla v) - b_h^E(\nabla w, \boldsymbol{\eta}) - b_h^E(\boldsymbol{\theta}, \nabla v) + b_h^E(\boldsymbol{\theta}, \boldsymbol{\eta}), \tag{14}$$

where the first term $b_h^E(\nabla w, \nabla v)$ can be calculated using the similar way for computation of $a_h^E(\boldsymbol{\theta}_h, \boldsymbol{\eta}_h)$. The derived consistent stiffness matrix $\boldsymbol{K}_{bw}^c$ and stability stiffness matrix $\boldsymbol{K}_{bw}^s$ are written as

$$\boldsymbol{K}_{bw}^c = \boldsymbol{\pi}_w^T \left\{ \int_E (\nabla \boldsymbol{N}_p^w)^T \boldsymbol{D}_s (\nabla \boldsymbol{N}_p^w) dE \right\} \boldsymbol{\pi}_w, \tag{15}$$

$$\boldsymbol{K}_{bw}^s = \tau tr(\boldsymbol{K}_{bw}^c)(\boldsymbol{I} - \boldsymbol{D}_w \boldsymbol{\pi}_w)^T (\boldsymbol{I} - \boldsymbol{D}_w \boldsymbol{\pi}_w). \tag{16}$$

The fourth term $b_h^E(\boldsymbol{\theta}, \boldsymbol{\eta})$ is computed through an equivalent projection operator Π_r^0 as introduced in [1], and the derived stiffness matrix $\boldsymbol{K}_{br}^c$ and stability stiffness matrix $\boldsymbol{K}_{br}^s$ are given as

$$\boldsymbol{K}_{br}^c = \boldsymbol{\pi}_r^{0T} \int_E (\nabla \boldsymbol{N}_p^r)^T \boldsymbol{D}_s (\nabla \boldsymbol{N}_p^r) dE \boldsymbol{\pi}_r^0, \tag{17}$$

$$\boldsymbol{K}_{br}^s = \tau tr(\boldsymbol{K}_{br}^c)(\boldsymbol{I} - \boldsymbol{D}_r \boldsymbol{\pi}_r^0)^T (\boldsymbol{I} - \boldsymbol{D}_r \boldsymbol{\pi}_r^0). \tag{18}$$

The third term $b_h^E(\boldsymbol{\theta}, \nabla v)$ is the symmetric part of the second term $b_h^E(\nabla w, \boldsymbol{\eta})$, which can be computed using the rule of integration by parts as

$$b_h^E(\nabla w, \boldsymbol{\eta}) = \int_e w^T \boldsymbol{\eta} \boldsymbol{n} de - \int_E w^T \nabla \boldsymbol{\eta} dE = \bar{\boldsymbol{w}} \boldsymbol{K}_{wr} \bar{\boldsymbol{\eta}}. \tag{19}$$

Note that w is a polynomial of $k+1$ and $\boldsymbol{\eta}$ is the polynomial of k. Therefore the term $\int_{\partial E} w^T \boldsymbol{\eta} \boldsymbol{n} d\partial E$ can be obtained by computing the integrations on the $k+2$ Gauss-Lobatto quadrature points (edge DOFs), and the term $\int_E w^T \nabla \boldsymbol{\eta} dE$ can be calculated by using the face DOFs predefined for the space $\mathcal{W}_h^{k+1}(E)$.

Eventually the stiffness matrix induced by bilinear forms $a_h^E(\boldsymbol{\theta}_h, \boldsymbol{\eta}_h)$ and $b_h^E(\boldsymbol{\theta} - \nabla w, \boldsymbol{\eta} - \nabla v)$ can be expressed as

$$\boldsymbol{K} = \begin{bmatrix} \boldsymbol{K}_{bw}^c + \boldsymbol{K}_{bw}^s & \boldsymbol{K}_{wr} \\ \boldsymbol{K}_{wr}^T & \boldsymbol{K}_a^c + \boldsymbol{K}_a^s + \boldsymbol{K}_{br}^c + \boldsymbol{K}_{br}^s \end{bmatrix}. \tag{20}$$

(a) Mesh $\mathcal{T}_1$ (b) Mesh $\mathcal{T}_2$ (c) Mesh $\mathcal{T}_3$ (d) Mesh $\mathcal{T}_4$
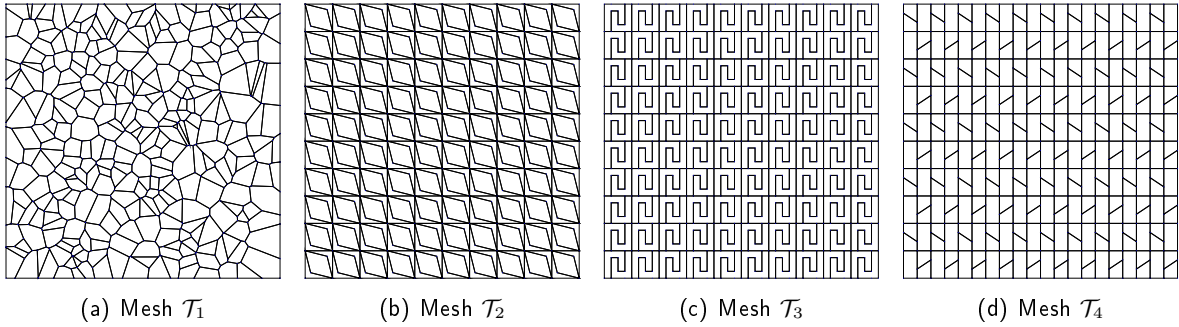
Figure 1: Four different types of mesh discretization for the unit square plate.

The external force vector $\boldsymbol{F}$ can be computed using the scheme presented in [15]. Then the displacement $\boldsymbol{u}$ consisting of deflection $\boldsymbol{w}$ and rotations $\boldsymbol{\theta}$ could be calculated by solving the system of equation

$$\boldsymbol{K}\,\boldsymbol{u} = \boldsymbol{F} \quad \Rightarrow \quad \boldsymbol{u} = \begin{Bmatrix} \boldsymbol{w} \\ \boldsymbol{\theta} \end{Bmatrix} = \boldsymbol{K}^{-1}\boldsymbol{F}. \tag{21}$$

Once the displacements are obtained, the pseudo stresses $\boldsymbol{\sigma}^p(\boldsymbol{u})$ can be computed by

$$\boldsymbol{\sigma}^p(\boldsymbol{u}) = \begin{Bmatrix} M_x & M_y & M_{xy} \end{Bmatrix}^T = \boldsymbol{D}_b\boldsymbol{\epsilon}^p = \boldsymbol{D}_b\partial\boldsymbol{N}_p^r\boldsymbol{\pi}_r\boldsymbol{\theta}. \tag{22}$$

4 NUMERICAL EXAMPLES

4.1 Square Plate

A benchmark problem is studied in this example to verify the robustness and convergence of the developed method on static bending analysis of Reissner-Mindlin plates. Consider a clamped unit square plate $\Omega \in [0,1]^2$ subjected to a transverse load g with the expression

$$\begin{aligned} f(x,y) = &\frac{E}{12(1-\nu^2)}[12y(y-1)(5x^2-5x+1)(2y^2(y-1)^2+x(x-1)(5y^2-5y+1)) \\ &+ 12x(x-1)(5y^2-5y+1)(2x^2(x-1)^2+y(y-1)(5x^2-5x+1))]. \end{aligned}$$

The analytical solutions of vertical displacement and rotations are given by

$$\begin{aligned} w(x,y) = &\frac{1}{3}x^3(x-1)^3y^3(y-1)^3 - \frac{2t^2}{5(1-\nu)}[y^3(y-1)^3x(x-1)(5x^2-5x+1) \\ &+ x^3(x-1)^3y(y-1)(5y^2-5y+1)], \\ \theta_x(x,y) = &x^3(x-1)^3y^2(y-1)^2(2y-1), \\ \theta_y(x,y) = &y^3(y-1)^3x^2(x-1)^2(2x-1). \end{aligned}$$

The material parameters are taken as: $E = 10.92 \times 10^6, \nu = 0.3, t = 0.1$. Some studies of this benchmark problem can be found in [16, 8, 12].

We first test the robustness of the developed method by using four different types of mesh discretizations with poor mesh qualities as provided in Fig 1. Mesh $\mathcal{T}_1$ is a voronoi diagram generated by a series of random

points. Mesh $\mathcal{T}_2$ consists of both concave polygonal elements and convex polygonal elements. Mesh $\mathcal{T}_3$ only consists of concave polygonal elements and some "hanging" nodes are designed for mesh $\mathcal{T}_4$. The obtained numerical results are plotted in Fig .2 where three rows correspond to vertical displacement w, rotation θ_x and bending moment M_x, and four columns are related to four mesh types. Note that p_w^3/p_r^2 virtual element method is used for these tests. Here p_w^{k+1}/p_r^k is used to state that the vertical displacement is interpolated with functions of degree $k+1$ and rotations are interpolated with functions of degree k. It can be found that the results qualitatively agree well with each other from the color plots.
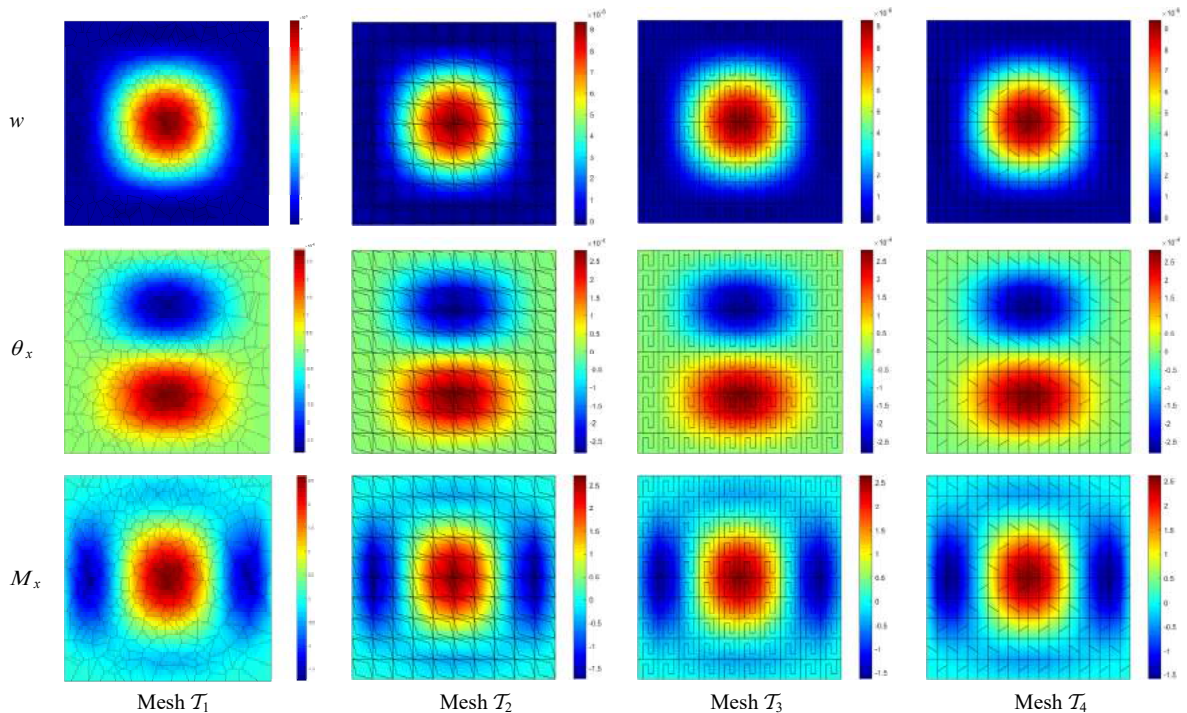
Figure 2: Plots of numerical results for the four types of mesh discretization. Top row: Vertical displacement w; Middle row: Rotation θ_x; Bottom row: Bending moment M_x.

Next we investigated the convergence of the method, for which an L_2-like relative error e_h^w for the vertical displacement is defined as

$$(e_h^w)^2 = \frac{\sum_{E \in \mathcal{T}_h} \int_E (w_{ex} - \Pi w_h)^2 dE}{\sum_{E \in \mathcal{T}_h} \int_E w_{ex}^2 dE}.$$

The error for rotations can be similarly defined by substituting $\boldsymbol{\theta}$ for w. To better describe the mesh size and compute the errors, we discretize the square plate into structured rectangular mesh. Figure 3 presents the relative errors e_w and e_{θ_x} with respect to mesh size h under three cases: $p_w^2/p_r^1, p_w^3/p_r^2, p_w^4/p_r^3$. The convergence rates for each curve are obtained from the last two data points and posted in Fig. 3. It is observed that both the vertical displacement w and rotation θ_x could achieve high convergence rates.
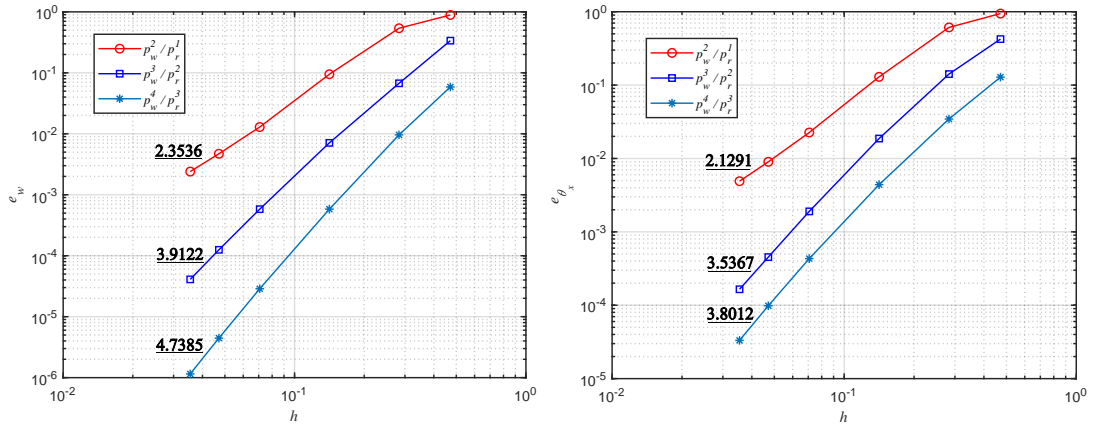
Figure 3: Relative errors of vertical displacement (Left) and rotation θ_x (Right) with respect to mesh size.

4.2 Cantilever Beam with a Circular Hole

In the second example, we consider the bending problem of a cantilever beam with a circular hole, studied in [12] by using non-conforming isogeometric analysis. Figure 4 provides the geometry and dimensions of the cantilever beam. The bottom edge is clamped and the top surface is subjected to a uniform load $q = -10$. Thickness $t = 50$, Young's modulus $E = 1 \times 10^{10}$ and Poisson ratio $\nu = 0.3$.
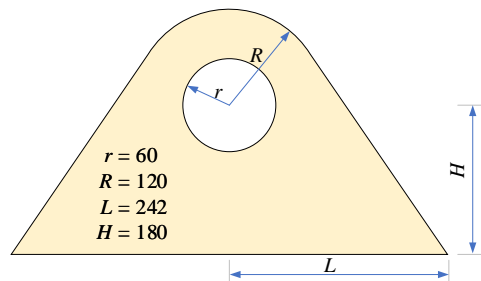
Figure 4: Geometry and dimensions of the cantilever beam with a circular hole.

Take the advantages of the insensitivity of elemental distortion and the permission of hanging nodes in VEM, we employ a simple mesh generation scheme to generate polygonal elements as shown in Fig. 5. First, the outer and inner boundary curves of the beam are defined and an initial background grid with 20×14 quadrilateral elements is then constructed according to the bounding box of the boundary curves. Note that the background grid does not have to be consistent with any types of the bounding box. Second, the elements intersecting with the boundary curves are refined by using a quadtree scheme to better capturing the boundary shapes. The elements in the background grid can be classified into three types: void elements, valid elements and trimmed elements. The void elements are located in the interior of the inner boundaries or exterior of the outer boundary. The valid elements are between the outer boundary and inner boundaries. The trimmed elements intersect with the boundary curves. In the last, the void elements are deleted and valid elements are reserved. The trimmed elements are converted to polygonal elements based on the intersection of the
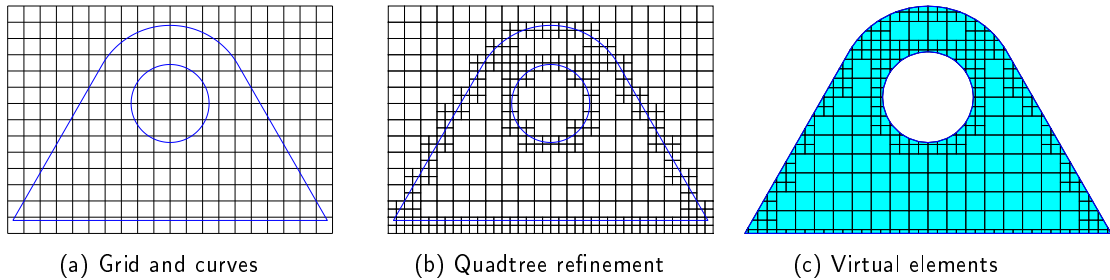
(a) Grid and curves   (b) Quadtree refinement   (c) Virtual elements

Figure 5: Generation of virtual elements for the cantilever beam based on the background grid and the quadtree refinement scheme.

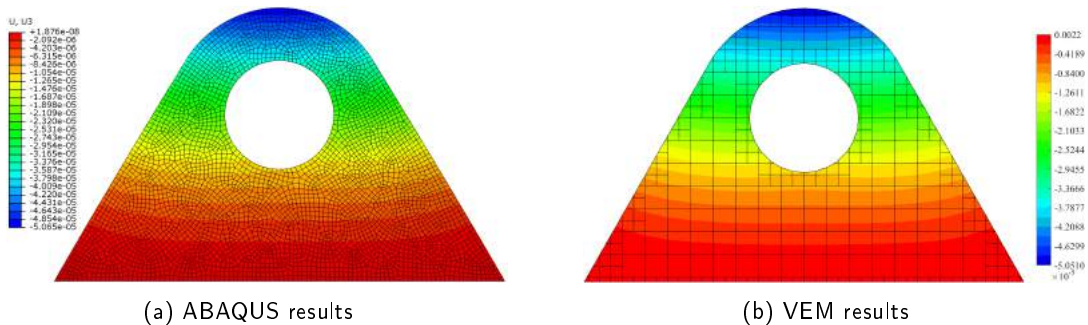(a) ABAQUS results   (b) VEM results

Figure 6: Comparison of deflection results obtained by using FEM and VEM.

boundary curves and elements. The valid elements and converted polygonal elements consist of the mesh for VEM. Figure 6 presents the deflection of the cantilever beam obtained by using commercial software ABAQUS and the proposed VEM of degree p_w^2/p_r^1. It can be found that the results agree very well with each other from the color plots.

4.3   Square Plate with Multiple Holes

A square plate with twelve inner trimmed holes subjected to a uniform load is studied in this example. Figure 7 illustrates the geometry and dimensions of the plate with multiple holes. Four edges of the plate are clamped and the load $q = -1$. Thickness $t = 15$, Young's modulus $E = 200 \times 10^6$ and Poisson ratio $\nu = 0.3$. Similar to the above example, the polygonal mesh is generated by using a quadtree refinement scheme and background grid as provided in Fig. 8. The grid is discretized into 12×12 elements. The elements that intersect with boundary curves are refined and the refinement depth is 2. In addition, the central elements are also refined to obtained better results. The obtained polygonal mesh as shown in Fig. 8c contains 616 elements and 925 nodes.

Using proposed VEM with polynomials of degree p_w^3/p_r^2 and the constructed mesh given in Fig. 8c, the deflection, rotation θ_x and moment M_x are obtained and plotted in Fig. 9. To validate the obtained results, the problem is also solved in ABAQUS using 3921 quadratic quadrilateral elements of type S8R and 12252 nodes. The deflection with respect to the x coordinates at section A-A (presented in Fig. 7) obtained by using the proposed VEM and FEM in ABAQUS are compared as shown in Fig. 10. It can be observed that both deflections show good agreements.
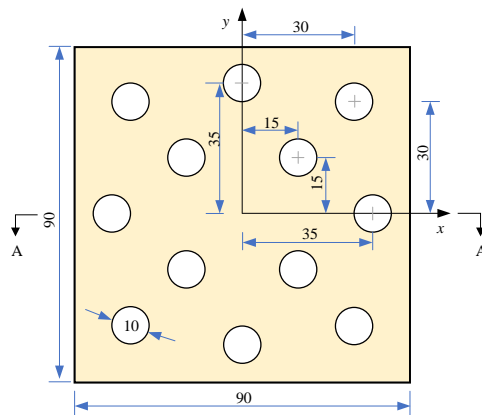
Figure 7: Geometry and dimensions.

(a) Grid and curves   (b) Quadtree refinement   (c) Virtual elements

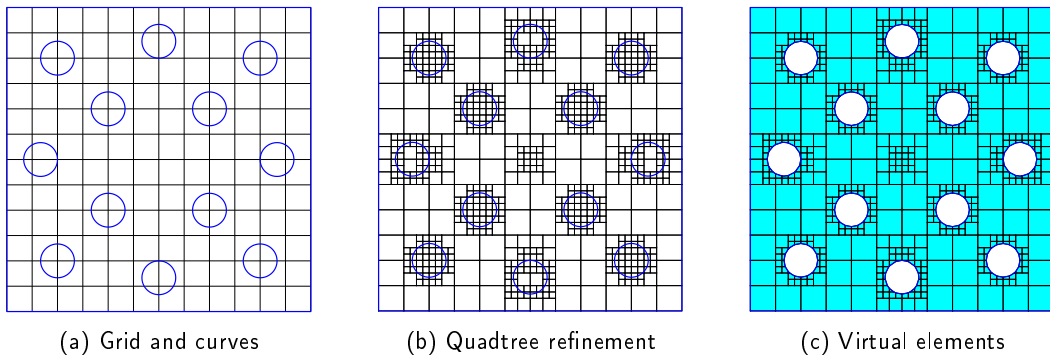**Figure 8**: Generation of virtual elements for the square plate with multiple holes based on the background grid and the quadtree refinement scheme.
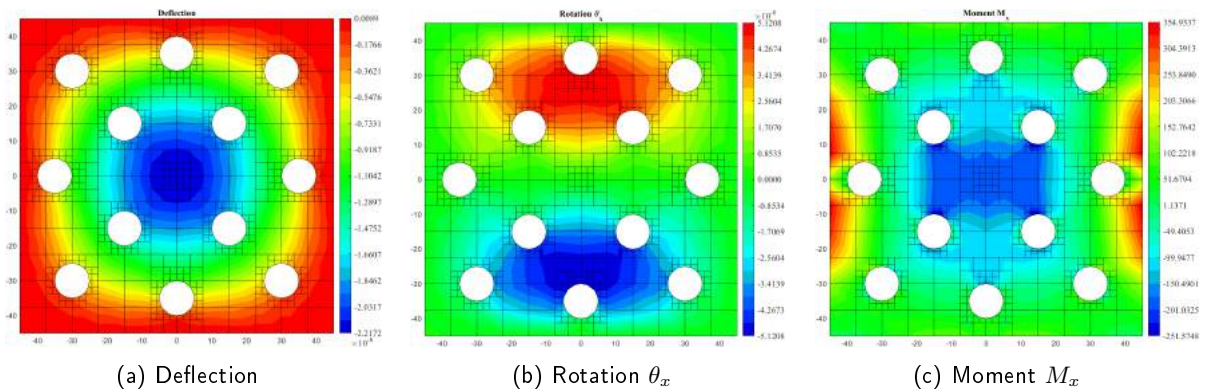

(a) Deflection   (b) Rotation θ_x (c) Moment M_x

Figure 9: Color plots of deflection, rotation θ_x and moment M_x of the multi-hole plate using virtual element method of degree 2.
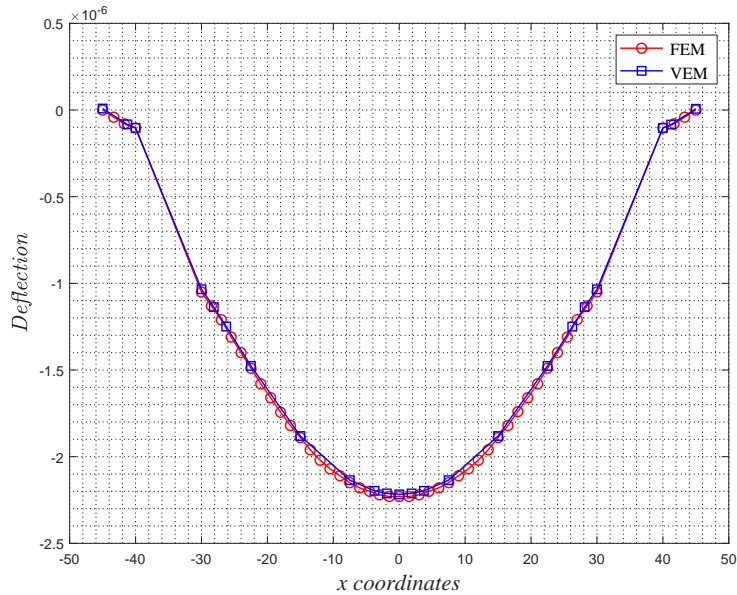
Figure 10: Comparison of the deflection at the secion A-A obtained by using the proposed VEM and FEM in ABAQUS.

5 CONCLUSIONS

Virtual element methods possess some appealing features including robustness to arbitrarily shaped polytopal discretizations and flexibility in dealing with non-conforming meshes. In this paper, a novel virtual element method is developed for static bending analysis of Reissner-Mindlin plate by using k-degree functions for interpolation of rotations and $(k+1)$-degree for interpolation of vertical displacement. The Reissner-Mindlin formulation is written in its primary form and none of the reduction operators or shear strains are used. The numerical results show the robustness and high convergence rates for the deflection and rotations. We note that the currently developed method is only valid for moderately thick plates and the numerical results for thin plates are still plagued by the shear locking phenomenon, which should be a good topic for future studies. The local refinement scheme employed in the last two examples shows the flexibility of VEM on handing polygonal elements and hanging nodes. Additionally, it is interesting to explore the improvement introduced by the local refinement of VEM based on the classical quadtree or octree refinement schemes.

ACKNOWLEDGEMENTS

Xiaoxiao Du, http://orcid.org/0000-0002-2324-1005

REFERENCES

[1] Ahmad, B.; Alsaedi, A.; Brezzi, F.; Marini, L.D.; Russo, A.: Equivalent projectors for virtual element methods. Computers & Mathematics with Applications, 66(3), 376–391, 2013. http://doi.org/10.1016/j.camwa.2013.05.015.

[2] Antonietti, P.F.; Bruggi, M.; Scacchi, S.; Verani, M.: On the virtual element method for topology optimization on polygonal meshes: a numerical study. Computers & Mathematics with Applications, 74(5), 1091–1109, 2017. http://doi.org/10.1016/j.camwa.2017.05.025.

[3] Arnold, D.N.; Brezzi, F.; Falk, R.S.; Marini, L.D.: Locking-free reissner–mindlin elements without reduced integration. Computer methods in applied mechanics and engineering, 196(37-40), 3660–3671, 2007. http://doi.org/10.1016/j.cma.2006.10.023.

[4] Artioli, E.; Da Veiga, L.B.; Dassi, F.: Curvilinear virtual elements for 2d solid mechanics applications. Computer Methods in Applied Mechanics and Engineering, 359, 112667, 2020. http://doi.org/10.1016/j.cma.2019.112667.

[5] Artioli, E.; da Veiga, L.B.; Lovadina, C.; Sacco, E.: Arbitrary order 2d virtual elements for polygonal meshes: part i, elastic problem. Computational Mechanics, 60(3), 355–377, 2017. http://doi.org/10.1007/s00466-017-1404-5.

[6] Brezzi, F.; Bathe, K.J.; Fortin, M.: Mixed-interpolated elements for reissner–mindlin plates. International Journal for Numerical Methods in Engineering, 28(8), 1787–1801, 1989. http://doi.org/10.1002/nme.1620280806.

[7] Chi, H.; Pereira, A.; Menezes, I.F.; Paulino, G.H.: Virtual element method (vem)-based topology optimization: an integrated framework. Structural and Multidisciplinary Optimization, 62(3), 1089–1114, 2020. http://doi.org/10.1007/s00158-019-02268-w.

[8] Chinosi, C.: Virtual elements for the reissner-mindlin plate problem. Numerical Methods for Partial Differential Equations, 34(4), 1117–1144, 2018. http://doi.org/10.1002/num.22248.

[9] Da Veiga, L.; Mora, D.; Rivera, G.: Virtual elements for a shear-deflection formulation of reissner–mindlin plates. Mathematics of Computation, 88(315), 149–178, 2019. http://doi.org/10.1090/mcom/3331.

[10] da Veiga, L.B.; Brezzi, F.; Cangiani, A.; Manzini, G.; Marini, L.D.; Russo, A.: Basic principles of virtual element methods. Mathematical Models and Methods in Applied Sciences, 23(01), 199–214, 2013. http://doi.org/10.1142/S0218202512500492.

[11] Da Veiga, L.B.; Buffa, A.; Lovadina, C.; Martinelli, M.; Sangalli, G.: An isogeometric method for the reissner–mindlin plate bending problem. Computer Methods in Applied Mechanics and Engineering, 209, 45–53, 2012. http://doi.org/10.1016/j.cma.2011.10.009.

[12] Du, X.; Zhao, G.; Wang, W.: Nitsche method for isogeometric analysis of reissner–mindlin plate with non-conforming multi-patches. Computer Aided Geometric Design, 35, 121–136, 2015. http://doi.org/10.1016/j.cagd.2015.03.005.

[13] Hughes, T.J.: The finite element method: linear static and dynamic finite element analysis. Prentice-Hall, 1987.

[14] Meng, J.; Mei, L.: A mixed virtual element method for the vibration problem of clamped kirchhoff plate. Advances in Computational Mathematics, 46(5), 1–18, 2020. http://doi.org/10.1007/s10444-020-09810-1.

[15] Mengolini, M.; Benedetto, M.F.; Aragón, A.M.: An engineering perspective to the virtual element method and its interplay with the standard finite element method. Computer Methods in Applied Mechanics and Engineering, 350, 995–1023, 2019. http://doi.org/10.1016/j.cma.2019.02.043.

[16] Mu, L.; Wang, J.; Ye, X.: A weak galerkin method for the reissner–mindlin plate in primary form. Journal of Scientific Computing, 75(2), 782–802, 2018. http://doi.org/10.1007/s10915-017-0564-y.

[17] Nguyen-Thanh, V.M.; Zhuang, X.; Nguyen-Xuan, H.; Rabczuk, T.; Wriggers, P.: A virtual element method for 2d linear elastic fracture analysis. Computer Methods in Applied Mechanics and Engineering, 340, 366–395, 2018. http://doi.org/10.1016/j.cma.2018.05.021.

[18] Wriggers, P.; Rust, W.T.: A virtual element method for frictional contact including large deformations. Engineering Computations, 36(7), 2133–2161, 2019. http://doi.org/10.1108/EC-02-2019-0043.

[19] Ye, X.; Zhang, S.; Zhang, Z.: A locking-free weak galerkin finite element method for reissner–mindlin plate on polygonal meshes. Computers & Mathematics with Applications, 80(5), 906–916, 2020. http://doi.org/10.1016/j.camwa.2020.05.015.